Disulfide Bond Mapping of Follitropin Delta, a Recombinant Follicle Stimulating Hormone (rFSH), at Atomic Resolution by X-Ray Crystallography

Dorin Kalson [*,†], Jeremiah S. Joseph [†], Hila Nudelman, Eyal Kamhi, Shlomo Bakshi

Posted Date: 27 January 2026

doi: 10.20944/preprints202601.1983.v1

Keywords: rFSH; di-sulfide bond; crystallography; X-ray

 doi:10.20944/preprints202601.1983.v1

Article

Disulfide Bond Mapping of Follitropin Delta, a Recombinant Follicle Stimulating Hormone (rFSH), at Atomic Resolution by X-Ray Crystallography

Dorin Kalson [1,*,†], Jeremiah S. Joseph [2,†], Hila Nudelman [1], Eyal Kamhi [1] and Shlomo Bakshi [1]

[1] Bio-Technology General Ltd

[2] Opilio LLC

* Correspondence: doka1@ferring.com

[†] These authors contributed equally to this work.

Abstract

Background/Objectives: Follitropin delta is an approved recombinant follicle stimulating hormone (rFSH) expressed in a human cell line. The FSH protein is a heterodimer containing α and β subunits. The FSH α-subunit (FSHα) contains five intramolecular disulfide bonds: C7-C31, C10-C60, C28-C82, C32-C84 and C59-C87. The α subunit has four closely spaced cysteine residues that form disulfide bonds. These clustered sites resist protease cleavage, making it difficult to accurately characterize the disulfide bond pairing in this type of protein therapeutic. **Methods**: The study uses an X-ray crystallography method to determine a high-resolution three-dimensional model structure of the recombinant FSH α-subunit. **Results**: The crystal structure of FSHα at 2.29 Å resolution, containing the disulfide bonds, is presented. This high-resolution structure provides definitive structural evidence that the disulfide bonds in rFSH are consistent with the expected native structural conformation. **Conclusions**: The rFSH structure validates the expected cysteine connectivity, overcoming limitations of prior mass spectrometry-based disulfide mapping attempts.

Keywords: rFSH; di-sulfide bond; crystallography; X-ray

1. Introduction

Follicle-stimulating hormone (FSH) is a heterodimeric glycoprotein hormone produced by the anterior pituitary gland in response to gonadotropin-releasing hormone (GnRH). FSH functions via the FSH receptor (FSHR), a G-protein-coupled receptor which is expressed mainly in female Granulosa cells (GC) and male Sertoli cells [1]. In females, FSH stimulates recruitment and growth of antral follicles by binding to its cognate receptor, FSHR, expressed on GC. Upon ligand binding, FSHR stimulates cyclic adenosine-monophosphate (cAMP) mediated signal transduction pathways inducing proliferation, differentiation and function of antral follicles as well as aromatase activity affecting steroidogenesis [2]. FSHR expression on GC increases upon FSH binding and its expression is affected by several other factors including estrogens, fibroblast growth factor, epidermal growth factor, and others. In addition, GC produces inhibins and activins in an FSH dependent manner further affecting FSHR expression, and hence FSH activity using an autocrine mechanism.

Disulfide bridges are covalent linkages formed between the thiol groups of two cysteine residues within a protein. These bonds play a pivotal role in maintaining protein stability and facilitating proper folding [3]. The thiol (-SH) group of cysteine is highly reactive, enabling the formation of disulfide bonds that contribute significantly to the structural integrity of proteins.

These bridges can be found within both the secondary and tertiary levels of protein structure. In the secondary structure, disulfide bonds help stabilize elements such as alpha helices and beta sheets by providing rigid connections that resist unfolding. At the tertiary level, they are essential for preserving the overall three-dimensional conformation of the protein. Disulfide bonds often link

 doi:10.20944/preprints202601.1983.v1

cysteine residues located in distant regions of the polypeptide chain, thereby anchoring different parts of the molecule and reinforcing its spatial arrangement [4].

FSH is composed of two non-covalently associated subunits, alpha (α) and beta (β). The α -subunit, is common to other gonadotropins, Luteinizing hormone (LH) and Choriogonadotropin (CG), and consists of 92 amino acids. The 111 amino acid β -subunit is specific to FSH and hence mediates specific binding and activation of FSH activity. Both FSH subunits carry N-linked glycosylations, at two positions: N52 and N78 for the α subunit and N7 and N24 for the β subunit [5]. Structurally, the two subunits have disulfide bonds [6] that covalently link the two parts of protein, forming the hydrophobic core of the protein. These disulfide bonds stabilize protein structure, help protein folding, and regulate protein function through a redox reaction. The FSHα subunit contains ten conserved cysteine residues forming five disulfide linkages (C7-C31, C10-C60, C28-C82, C32-C84 and C59-C87. These disulfide linkages are depicted in Figure 1.

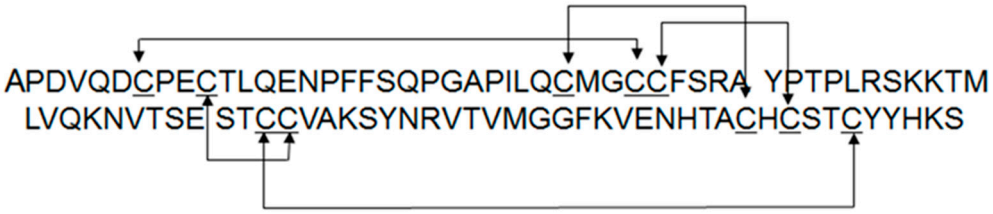

Figure 1. The structure of FSH α-subunit (FSHα) contains five intramolecular disulfide bonds: C7-C31, C10-C60, C28-C82, C32-C84 and C59-C87.

The α subunit contains four closely spaced cysteine residues at positions Cys31, Cys32, Cys59, and Cys60, which form disulfide bonds with other cysteines. These tightly clustered sites are resistant to efficient cleavage by specific proteases, making accurate disulfide bond characterization in the α subunit especially challenging for this class of protein therapeutics. The disulfide bond characterization of the α subunit is rarely reported for native rFSH due to significant technical challenges.

Traditionally, mass spectrometry-based peptide mapping has been employed to elucidate disulfide bond patterns [7]. However, the challenge of identifying FSH disulfide bonds arises from the lack of a specific and optimal protease capable of selectively cleaving peptides between closely spaced disulfide bonds. Additionally, peptides often contain more than two cysteines, making it difficult to pinpoint exact linkage sites. Methods involving reduction or partial reduction to selectively break disulfide bonds are also difficult to control reliably.

Follitropin delta (Rekovelle®), which was approved in Europe in 2016 [8–10], is the first recombinant FSH protein expressed in the human fetal retinal cell-line PER.C6®. To this end, PER.C6® cells were genetically engineered to express the human FSH α and β genes and, in addition, the human α 2,3-sialyltransferase (ST3) enzyme to facilitate improved sialylation [11].

In this study, the strategy of X-ray crystallography was used to determine the high-resolution three-dimensional structure of the Follitropin delta α-subunit. By directly visualizing the electron density map associated with disulfide linkages in FSHα within the crystal structure, we aimed to provide definitive structural evidence that the disulfide bonds in the recombinant material are consistent with the expected native configuration. This structural validation is intended to support regulatory submissions by demonstrating correct and intact disulfide bonding in the recombinant FSH preparation.

 doi:10.20944/preprints202601.1983.v1

2. Materials and Methods

2.1. Protein Production

Recombinant FSH: Two batches of recombinant human FSH, produced in PER.C6® cells at Bio-Technology General (Israel) Ltd., were used in this study. The samples were stored and transferred at -20°C degrees, in a formulation buffer of 1 mM Na2HPO4·12H2O with 0.5 mg/mL L-Methionine and 0.005 mg/mL Polysorbate 20, pH 6.75±0.2, at 0.63 mg/mL concentration.

Due to the difficulty in removing FSH glycans with PNGase F, a pan-sialidase (Lectenz Bio, catalog No. GE0701) was used to enzymatically remove terminal sialic acid residues. This step served to reduce heterogeneity and the overall negative surface charge, thereby improving crystallizability. One 5,000-unit vial of sialidase was used per 10 mg of FSH, and digestion was monitored by reducing and non-reducing SDS-PAGE. The desialylated protein was concentrated to 5.6 mg/mL in 20 mM HEPES pH 7.5, 100 mM NaCl and used directly for complex formation.

Anti-FSHα Fab: As a strategy to aid crystallization, an anti-FSHα Fab fragment was engineered based on the sequence of the Fv structure in PDB 1QFW [12]. An Ala12Ser mutation (mature light chain numbering; Table 1) was introduced into the Fab light chain construct to correct the only mismatch in the binding interface for the elbow-stabilizing anti-kappa VHH nanobody, based on PDB structure 8JH7 [13], which we additionally employed. This design ensured co-binding of the VHH to enhance lattice formation during crystallization.

Codon-optimized sequences of the Fab heavy and light chains were synthesized and cloned into pTT5 mammalian expression vectors. The constructs were co-transfected into Expi293F cells (1 L scale) and cultured at 37 °C. The supernatant was harvested 120 hours post-transfection.

The secreted Fab was purified by affinity chromatography using a CaptureSelect IgG-CH1 column. After washing with PBS, the Fab was eluted with 20 mM acetate pH 3.5, 150 mM NaCl, and immediately neutralized with 1 M Tris pH 8.0. The eluate was then purified by size exclusion column (SEC) on a Superdex 200 16/600 column equilibrated in 50 mM Tris pH 7.5, 150 mM NaCl. The purified Fab was concentrated and flash-frozen in liquid nitrogen for storage. Electrospray ionization mass spectrometry (ESI-MS) was used to confirm protein purity and consistency with the expected disulfide bond formation.

Anti-kappa VHH: To support Fab elbow stabilization and aid crystallization of the FSH/Fab complex, an anti-kappa nanobody (VHH) was produced. This single-domain VHH, derived from PDB structure 8JH7[13], specifically recognizes the constant region of the human kappa light chain.

A codon-optimized sequence of the anti-kappa VHH was cloned into a pET26b vector containing a pelB signal sequence and transformed into E. coli BL21(DE3) cells. A 2 L LB culture was grown at 37 °C to an OD600 of ~0.6 and induced with 0.1 mM IPTG. Expression continued at 16 °C for 48 hours.

Cells were harvested by centrifugation and resuspended in lysis buffer containing 20 mM HEPES pH 7.5, 100 mM NaCl, 10 mM imidazole, 5 mM $MgCl_2$, 1 mM PMSF, 50 µg/mL DNase I, 100 µg/mL lysozyme, and protease inhibitor tablets (1 per 50 mL). Lysis was performed by sonication, and the clarified lysate was applied to a Ni affinity column pre-equilibrated with Buffer A (20 mM HEPES pH 7.5, 500 mM NaCl, 40 mM imidazole). The column was washed extensively with Buffer A, and the bound VHH was eluted with Buffer B (20 mM HEPES pH 7.5, 100 mM NaCl, 500 mM imidazole).

The eluate was concentrated and further purified by SEC on a Superdex 75 16/600 column equilibrated in 10 mM HEPES pH 7.5, 100 mM NaCl, 10% glycerol. Peak fractions were pooled, concentrated, and flash-frozen in liquid nitrogen for storage. ESI-MS was used to confirm protein purity and consistency with the expected disulfide bond formation.

 doi:10.20944/preprints202601.1983.v1

Table 1. Expressed protein sequence.

Construct	Sequence
Anti-FSHα Fab LC	MKHLWFFLLLVAAPRWVLSDIELTQSPDSLSVSLGQRATISCRASESVDSYGNSFMQWY QQKPGQPKLLIYRASNLEGSIPARFSGTGSRTDFTLTINPVEADDVATYYCQQSDEYPYM YTFGGGTKLEIKRTVAAPSVFIFPPSDEQLKSGTASVVCLLNNFYPREAKVQWKVDNALQSGN SQESVTEQDSKDSTYSLSSTLTLSKADYEKHKVYACEVTHQGLSSPVTKSFNRGEC
Anti-FSHα Fab HC	MVLQTQVFISLLWISGAYGQVQLQQSGAELVKPGASVKLSCKASDYTFTSYWMHWVKQRP GQGLEWIGEINPTNGRTYYNEKFKSKATLTDVKSSSTAYMQLSSLTSEDSAVTTCATTYGNSFDY WGQGTTVTVSSASTKGPSVFPLAPSSKSTSGGTAALGCLVKDYFPEPVTVSWNSGALTSVHTFPA VLQSSGLYSLSSVVTVPSSSLGTQTYICNVNHKPSTNTKVDKKVEPKSCDKTHT
Anti-kappa VHH	MKYLLPTAAAGLLLLAAQPAMAHHHHHHQVQLQESGGGLVQPGGSLRLSCAASGRTISRYA MSWFRQAPGKEREFVAVARRSGDGAFYADSVQGRFTVSRDDAKNTVYLQMNSLKPEDTAYYCA IDSDTFYSGSYDYGWGQGTQVTVSS

*Signal peptide sequences are underlined.

2.2. Crystallization

FSH/Fab/VHH complex: A ternary complex was prepared by incubating 1.5 mg desialylated FSH (Batch A) with 4.83 mg Fab and 1.9 mg VHH on ice for two hours, followed by SEC purification as above. Peak fractions were pooled and concentrated to 7.3 mg/mL and used for crystallization screening.

Crystallization screening of each of these preparations was performed using the sitting-drop vapor diffusion method in a 96-well format at 18 °C. Each drop consisted of 150 nL protein solution mixed with 150 nL crystallant solution. Harvestable crystals were cryoprotected as needed and flash-cooled in liquid nitrogen and screened for X-ray diffraction.

Fine-screen conditions were explored around the original hit conditions that yielded well-diffracting crystals, with crystallization trials set up using the hanging-drop vapor diffusion method at 18 °C. Drops consisting of protein solution and crystallant solution were mixed at three different ratios: 1 µL + 2 µL, 1.5 µL + 1.5 µL, and 2 µL + 1 µL. Larger drop sizes were used to encourage growth of bigger, better diffracting crystals. Streak seeding with crystals from initial hits was applied to all drops to enhance nucleation and improve crystal quality. The optimized crystallization conditions were intrinsically cryoprotective and required no additional cryoprotectant. These optimized crystallization conditions yielding well-diffracting crystals for the ternary FSH/Fab/VHH complex were adapted and applied successfully to additional FSH batch (Batch B).

2.3. X-Ray Diffraction

Crystals were screened and complete diffraction datasets were collected at 100 K with a wavelength of 0.97918 Å from well-diffracting crystals of the FSH/Fab/VHH complex (Batch A), at the Shanghai Synchrotron Radiation Facility (SSRF, beam line BL10U2). Crystals were screened and complete diffraction datasets collected at 100 K with a wavelength of 0.97625 Å from well-diffracting crystals of the FSH/Fab/VHH complex (Batch B) at the Diamond Light Source (DLS beam line I03, UK).

2.4. Structure Determination

Diffraction images were processed automatically at the synchrotron beamlines using the xia2-dials 3dii pipeline. Merged and scaled intensities were obtained using AIMLESS.

Initial phases were obtained by molecular replacement using Phaser (within the Phenix suite), with search models including FSH (PDB: 1FL7), Fab (PDB: 7Fab), and VHH (from PDB: 3JH7). The model was manually built into interpretable electron density using Coot, with iterative cycles of model building and refinement carried out in Phenix and Coot.

Particular attention was given to disulfide bond connectivity. Electron density corresponding to cysteine residues was carefully inspected to confirm the presence and correct pairing of disulfide linkages. The final model was validated using MolProbity.

 doi:10.20944/preprints202601.1983.v1

3. Results

As a first step, recombinant human FSH from the two batches was analyzed by SDS-PAGE under both reducing and non-reducing conditions to assess purity, integrity, and disulfide-linked dimerization (Figure 2A). Under reducing conditions, the proteins migrated as two overlapping fuzzy bands corresponding to the glycosylated α and β subunits (~24–26 kDa), as expected for heavily glycosylated proteins. In contrast, non-reducing SDS-PAGE of unheated samples revealed a single band near ~40 kDa, consistent with the intact, disulfide-linked FSH heterodimer. Heating the samples prior to loading caused the heterodimer to dissociate into its component subunits, with mobilities similar to those of the reducing condition (Figure 2A).

To improve crystallization by minimizing glycosylation heterogeneity, we explored enzymatic strategies to simplify the glycans. Initial attempts to enzymatically deglycosylate Batch A using PNGase F and Endo H—individually and in combination—failed to shift the protein's mobility on SDS-PAGE (Figure 2B). This result suggested that the complex, sialylated glycan structures on mature FSH were resistant to cleavage by these enzymes, consistent with prior reports.

We next employed a bacterial pan-sialidase (Lectenz Bio, GE0701) to remove terminal sialic acids. This treatment resulted in a reproducible electrophoretic mobility shift and noticeable band sharpening under both reducing and non-reducing conditions (Figure 2C), indicative of successful sialic acid removal and improved protein homogeneity. These effects were consistent with both batches of FSH and were observed regardless of a heating status prior to electrophoresis. Unheated samples maintained the ~40 kDa band, while the heated, sialidase-treated samples dissociated into sharper ~24–26 kDa bands, confirming both sialidase efficacy and the integrity of the heterodimer under native conditions.

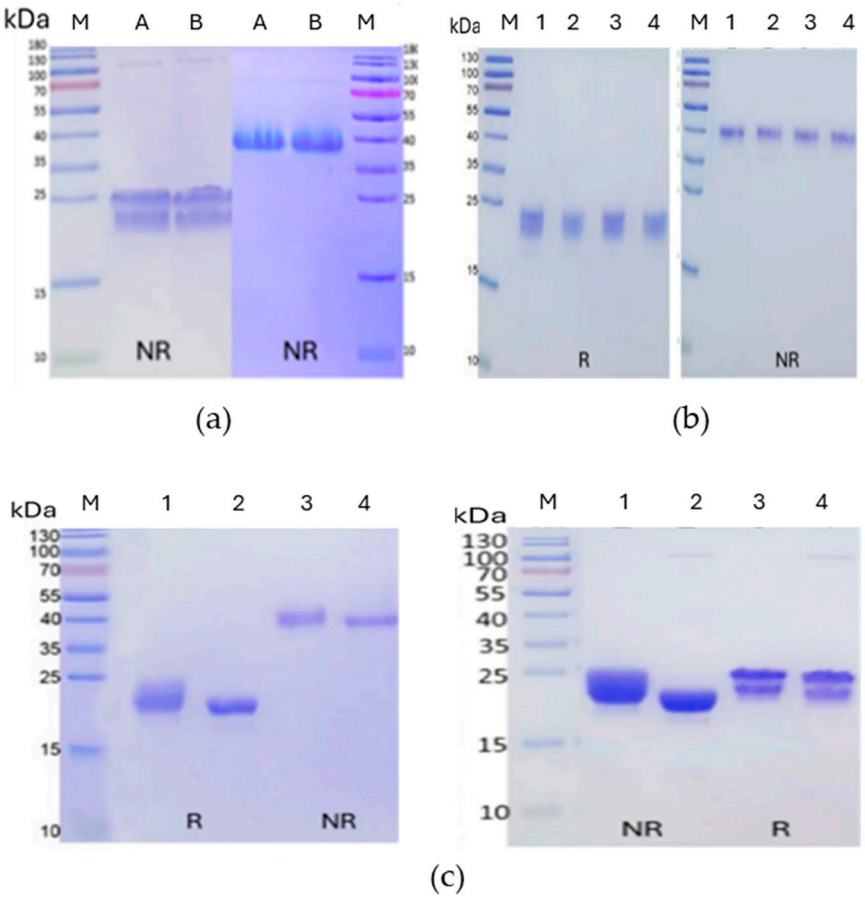

Figure 2. SDS-PAGE analysis of recombinant FSH. (a) Non-reducing SDS-PAGE gels of Batch A and Batch B heated (left panel) or unheated (right panel) prior to loading. Both batches look identical. The heated samples

 doi:10.20944/preprints202601.1983.v1

show bands (~24–26 kDa) consistent with glycosylated α and β subunits (left), and the non-heated samples show single ~40 kDa bands, corresponding to the intact FSH heterodimer (right). (b) Deglycosylation attempts on FSH batch A. (1) Untreated, (2) PNGase, (3) Endo H, (4) PNGase F +Endo H (4). No significant glycan removal was observed by mobility shifts on reducing (left) and non-reducing (right) SDS-PAGE gels. (c) Desialidation of FSH batches A (left) and B (right). Lanes 1 and 3 are untreated reduced and non-reduced samples, respectively; Lanes 2 and 4 are reduced and non-reduced samples treated with pan-sialidase. Batch A samples were unheated prior to gel loading while Batch B were heated. The clear mobility shift and narrowing of protein bands upon sialidase treatment suggest significant sialic acid removal and improvement in homogeneity of FSH.

Based on these results, desialylated FSH preparations from Batches A and B were selected for all subsequent crystallization experiments, either as isolated FSH or in complex with binding partners.

Crystallization trials with desialylated FSH alone yielded clusters of small needle-like crystals in a few conditions (data not shown). These crystals were not considered suitable for harvesting, their poor quality attributable to the inherent heterogeneity of glycosylation, which can impair crystal lattice formation. They were not pursued further. Instead, a crystallization chaperone strategy was employed, as described below.

FSH/anti-FSHα Fab/anti-kappa VHH

To aid in formation of diffraction quality crystals, an anti-FSHα Fab fragment was engineered based on the Fv molecule in PDB 1QFW [12], for use in a complex with FSH. Since Fabs are typically flexible at their elbow junction, a well-characterized anti-kappa elbow-binding nanobody (VHH) described in the literature [14], was employed to stabilize the FSH/Fab complex and enhance its crystallizability.

FSH formed a stable and well-behaved complex with the anti-FSHα Fab and the anti-kappa VHH, evidenced by a distinct, monodisperse peak on SEC (Figure 3).

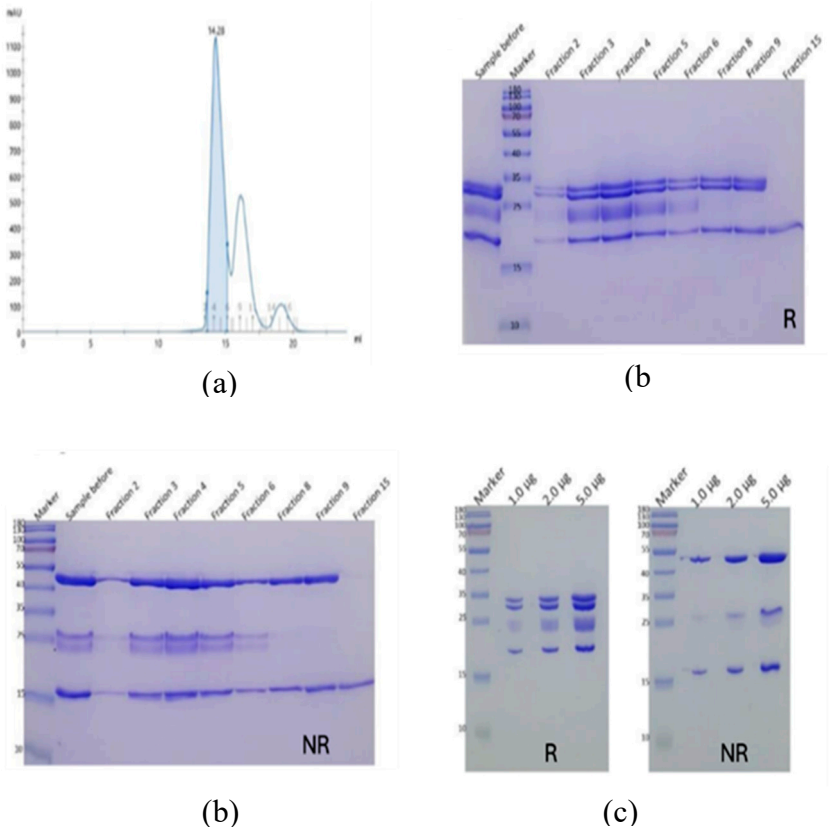

Figure 3. Complex formation of FSH (Batch A) with anti-FSHα Fab and anti-kappa VHH. FSH was incubated with Fab and VHH on ice for two hours, then the well-formed complex purified by SEC (a). SDSPAGE was used to assess SEC fractions (b) and the purified complex (c).

 doi:10.20944/preprints202601.1983.v1

Crystallization of the FSH/Fab/VHH ternary complex was carried out using the sitting-drop vapor diffusion method. Protein crystals appeared within three days (Figure 4), A protein crystal from a condition 0.05 M calcium chloride, 0.1 M Bis-Tris pH 6.5, 30% v/v PEG 550 MME, yielded high resolution diffraction of 2.53 Å with the space group P212121. Analysis was conducted using the 2.53 Å dataset, with the corresponding statistics presented in Table 2.

Figure 4. Crystallization of desialylated FSH (Batch A) in complex with anti-FSHα Fab and antikappa VHH. Sitting drop crystallization using 7.3 mg/ml protein yielded harvestable crystal at 18 °C in a condition of 0.05 M calcium chloride, 0.1 M Bis-Tris pH 6.5, 30% v/v PEG 550 MME. The representative image shown was photographed three days after setup.

The crystal structure (PDB:9YXD) was solved by molecular replacement (Table 2) using Phaser (Phenix suite), with search models for FSH (PDB: 1FL7), Fab (PDB: 7Fab), and VHH (PDB: 3JH7). The asymmetric unit contained one copy of the FSH/Fab/VHH complex (Figure 5), with a solvent content of 66.2%, consistent with a loosely packed but well-ordered lattice.

Model building proceeded iteratively, with manual adjustments guided by interpretable electron density maps. All regions were well resolved except for a flexible loop in the Fab heavy chain (residues S132–G137), and one in the Fab light chain (residues E27-S36) which lacked continuous density.

Table 2. Data collection, structure determination and refinement statistics for FSH (Batch A and Batch B) complex with anti-FSHα Fab and anti-kappa VHH. Data in parenthesis correspond to the highest resolution shell.

Data Collection & Refinement Statistics	Batch A	Batch B
Beamline	SSRF BL10U2	DLS I03
Wavelength (Å)	0.9792	0.97625
Resolution range (Å)	158.88–2.53 (2.63–2.53)	29.85-2.29 (2.35-2.29)
Space group	$P2_12_12_1$	$P2_12_12_1$
Unit cell parameters (Å; °)	a = 75.71, b = 102.47, c = 158.88; α = β = γ = 90	a = 76.01, b = 101.10, c = 161.24; α = β = γ = 90
Matthew coefficient (Å3/Da)	3.63	3.65
Molecules per asymmetric unit	1	1
Total reflections	548805 (58681)	739731 (40781)
Unique reflections	42007 (4344)	56196 (3969)
Multiplicity	13.1 (13.5)	13.2 (10.3)
Completeness (%)	100 (100)	98.6 (86.8)
Mean I/sigma(I)	9.7 (2.3)	33.8 (5.5)
Wilson B-factor	55.49	50.15

 doi:10.20944/preprints202601.1983.v1

R-merge/R-meas/Rpim	0.131 (1.066)/0.136 (1.109)/0.038 (0.301)	0.044 (0.29)/0.045 (0.305)/0.012 (0.093)
CC1/2	0.996 (0.866)	1 (0.966)
Reflections used in refinement	41669 (2740)	55871 (2341)
Reflections used for R-free	2031 (128)	2814 (131)
Rwork/Rfree	0.2207/0.2705	0.1947 (0.2284)
Total no. of non-hydrogen atoms (protein)	5978	6254
No. of protein/solvent residues	735/263	743/454
RMSD bond lengths, bond angles (Å; °)	0.009/1.15	0.007/0.95
Ramachandran favored/ allowed/ outliers/ rotamer outliers (%)	94.31/4.17/1.53/5.03	97.13/2.74/0.14/2.33
Clashscore	10.27	8.58
Average B-factor/protein/ligands/solvent	56.04/55.83/80.17/55.29	52.10/51.49/72.97/55.59

Crystal packing analysis revealed that each complex interacts with ten symmetry-related neighbors within 4 Å. These contacts include five FSH molecules, three Fabs, and four VHHs, indicating that all components participate in lattice formation (data not shown). The Fab and VHH, in particular, enhance the number and stability of packing interactions, acting as effective scaffolds that rigidify the complex and facilitate crystallization. All three resolved N-linked glycans—two in FSHβ and one in FSHα—extend into solvent channels and avoid interfering with symmetry contacts. This favorable glycan orientation likely contributed to the high quality of the diffraction data despite the inherent heterogeneity of the glycoprotein.

As shown in Figure 5, FSH adopts the expected architecture observed in previous structures: both α and β subunits form central cystine-knot motifs with three β-hairpin loops, assembling into a compact, elongated heterodimer stabilized by multiple disulfide bonds and polar interactions. The Fab binds to the same α-subunit epitope as its parental Fv (PDB: 1QFW), maintaining specificity. The engineered VHH engages the Fab light chain elbow, consistent with the 8JH7 structure, and was included to rigidify this otherwise flexible region. This design was successful; the complex was well ordered and formed a dense, cooperative lattice mediated by Fab and VHH interfaces.

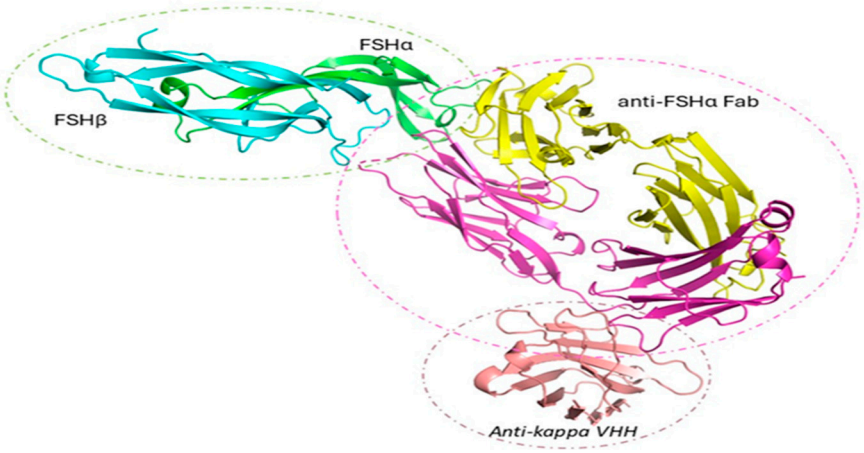

Figure 5. Crystal structure of the FSH/anti-FSHα Fab/anti-kappa VHH complex (Batch A). The asymmetric unit contains a single copy of the ternary complex comprising human FSH (α-subunit: green; β-subunit: cyan), the anti-FSHα Fab (heavy chain: yellow; light chain: magenta), and an elbow-stabilizing antikappa VHH (salmon). N-linked glycans (sticks) are shown at three resolved glycosylation sites.

 doi:10.20944/preprints202601.1983.v1

At 2.53 Å resolution, the electron density was of sufficient quality to definitively assign all disulfide bonds in the FSH α and β subunits (Figure 6). Each cysteine pairing was supported by continuous and unambiguous 2Fo–Fc density, validating the expected disulfide architecture. These observations provide clear experimental confirmation of the full disulfide connectivity in recombinant FSH.

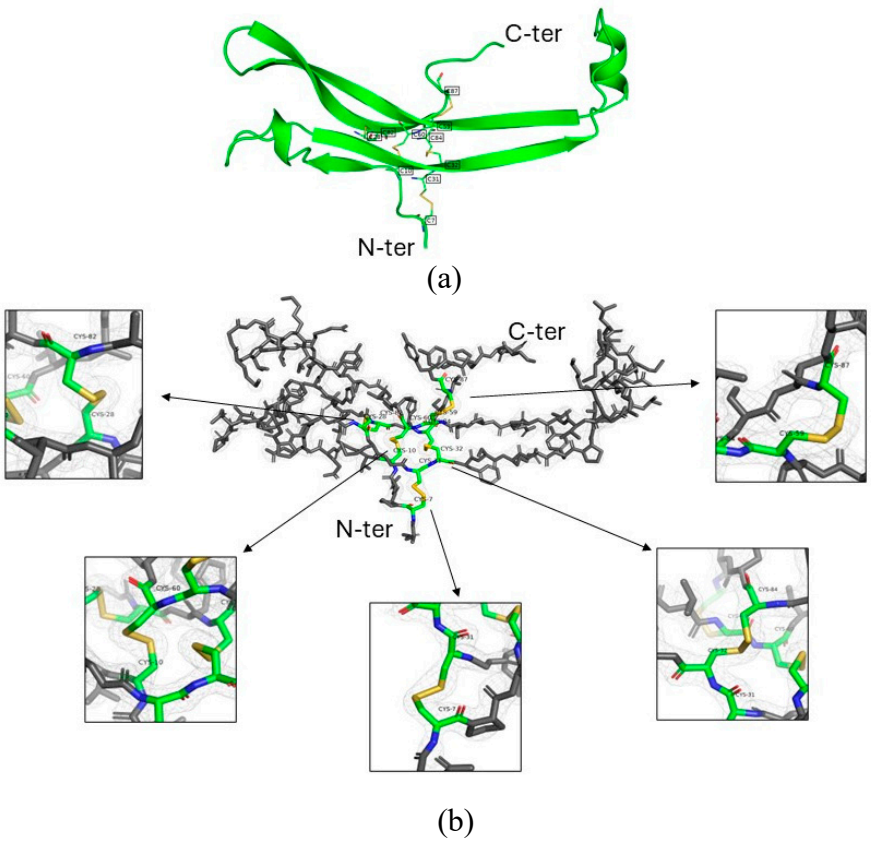

Figure 6. (a) Ribbon diagram of the follitropin delta α-subunit showing its secondary structure elements. The protein backbone is represented in green, highlighting β-strands forming sheets and a single α-helix. Disulfide bonds between cysteine residues (C7–C31, C10–C60, C28-C82, C32–C84, and C59–C87) are shown in yellow, with labeled cysteine positions ensuring structural stability of the glycoprotein hormone subunit. **(b)** Electron density around disulfide bonds in FSHα subunit from Batch A. The 2.53 Å 2Fo–Fc electron density shown contoured at 1.0 σ around the follitropin delta α-subunit and a zoom in on each disulfide bond allowed unambiguous assignment of canonical and intact S–S connectivity in this subunit.

Following successful optimization of crystallization conditions using Batch A, the same disulfide mapping strategy was applied to the additional Batch, B. Desialylated FSH (Figure 2) was complexed with anti-FSHα Fab and anti-kappa VHH to form the ternary complex. The complex was purified by SEC, yielding a single, monodisperse peak. Peak fractions were pooled and concentrated to a similar concentration as the Batch A complex (7.5 mg/mL) for crystallization. Crystallization trials were conducted using the hanging-drop vapor diffusion method at 18 °C, employing fine screens around the previously identified hit condition that produced well-diffracting crystals with Batch A: 0.05 M Calcium chloride, 0.1 M Bis-Tris pH 6.5, 30% v/v PEG 550 MME. The fine screen robustly produced large harvestable crystals (Figure 7).

 doi:10.20944/preprints202601.1983.v1

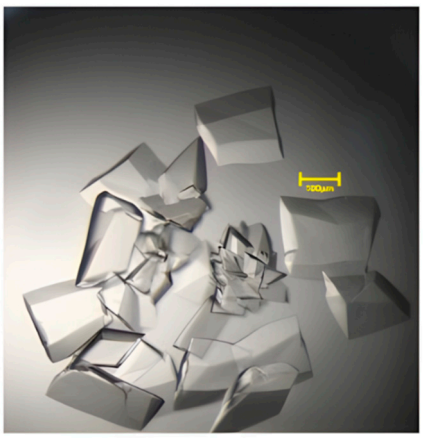

Figure 7. Crystallization of desialylated FSH (Batch B) in complex with anti-FSHα Fab and anti-kappa VHH. Hanging drop crystallization was performed using 7.5 mg/ml protein, with 3 ul drop sizes and streak seeding from previous crystals. This yielded large harvestable crystals at 18 °C. The representative images shown were taken four days after setup.

Six crystals were subjected to X-ray diffraction at the Diamond Light Source (BL I03). All six crystals diffracted well, and X-ray data processing indicated that all crystals belonged to the same orthorhombic space group ($P2_12_12_1$) with similar unit cell parameters.

One crystal was diffracted to the highest resolution of 2.29 Å which was selected for model refinement (Table 2).

All structural elements were well resolved except for a flexible loop in the Fab light chain (D30-Y21), which lacked continuous electron density. Extra density corresponding to all four N-linked glycans—two on FSHα and two on FSHβ — were observed at this resolution.

4. Discussion

Accurate disulfide mapping is a critical attribute for recombinant FSH products, as incorrect disulfide pairing can lead to misfolded or inactive protein, potentially affecting efficacy or immunogenicity [15]. Traditionally, mass spectrometry-based peptide mapping has been employed to elucidate disulfide bond patterns [16]. However, in our case, attempts at disulfide mapping using the isolated recombinant FSHα subunit were ultimately unsuccessful due to a combination of factors: the high number of cysteines, the resulting disulfide bonds in close proximity to each other and to glycosylated residues, susceptibility to disulfide scrambling during sample preparation, and incomplete peptide fragmentation under non-reducing conditions, and the complexity of glycosylation conferred by the host PER.C6® cells. Despite extensive efforts involving multiple rounds of proteolytic digestion, deglycosylation, and partial reduction strategies, the heavily glycosylated and compact nature of FSHα prevented confident disulfide bond assignment. These negative results led us to pursue X-ray crystallography as a definitive approach to resolve the disulfide topology of recombinant FSH under native conditions.

Literature offers a few structural precedents for glycoprotein hormones, with most relying on deglycosylation, desialylation, or protein engineering to improve lattice formation.

Only a single structure of native-like FSH in isolation has been reported (PDB: 1FL7), in which the hormone was produced in Trichoplusia ni (Hi5) insect cells and engineered to remove a β-subunit glycosylation site (T26A) to reduce heterogeneity and promote crystallization [17]. This strategy, while effective, is not compatible with clinical or GMP-grade material produced in mammalian cells. For our study, which focused on structurally validating a native recombinant FSH product, we could not alter glycosylation through genetic means.

Related strategies have been pursued with human chorionic gonadotropin (hCG), which shares the FSHα subunit and is similarly glycosylated. Early crystal structures of hCG (1HCN, 1HRP) were

 doi:10.20944/preprints202601.1983.v1

obtained after chemical deglycosylation with anhydrous hydrogen fluoride (HF) [18,19], a harsh treatment that can damage the protein backbone. Lustbader et al. [20] demonstrated that enzymatic desialylation using neuraminidase led to better crystal quality and reduced peptide bond cleavage compared to HF-treated samples. Their findings suggested that negatively charged terminal sialic acids, rather than total glycan content, are the principal inhibitors of lattice formation. Later, a ternary complex of fully glycosylated hCG and two Fv fragments was crystallized, which resulted in a structure, albeit at lower resolution (1QFW), highlighting the utility of crystallization chaperones in overcoming glycan-related barriers.

Taken together, the above challenges necessitated development of a crystallization strategy based on desialylation and engineered antibody fragments as auxiliary crystallization partners, that shielded or stabilized glycan-rich regions and promoted consistent packing, enabling high-resolution structure determination of native, unmodified recombinant FSH. To this end, recognizing the potentially high attrition rate (due to glycan heterogeneity, structural flexibility, and diffraction quality) multiple crystallization strategies were pursued for a ternary FSH/Fab/VHH complex, which yielded high-quality crystals with high resolution, leading to structures of 2.53 Å (FSH Batch A) and 2.29 Å (FSH batch B).

The structures revealed a single complex per asymmetric unit and extensive lattice interactions mediated predominantly by the Fab and VHH, which stabilized the architecture and enabled nucleation and crystal growth. Glycans projected into solvent channels, avoiding steric interference.

Critically, the excellent electron density maps obtained allowed unambiguous assignment of all five disulfide bonds in the FSHα subunit of the FSH heterodimer. The structural data validates the expected cysteine connectivity, overcoming limitations of prior mass spectrometry-based disulfide mapping. The structure provides a high-resolution reference for quality control, offering a direct and orthogonal method for unambiguously visualizing disulfide linkages within the context of the intact folded protein.

Author Contributions: Conceptualization, D.K., J.S.J. and S.B; methodology, D.K. and J.S.J; software, J.S.J; formal analysis, .J.S.J and D.K.; investigation, D.K. and J.S.J.; resources, D.K., S.B. and J.S.S.; data curation, D.K. and J.S.J; writing—original draft preparation, D.K., J.S.J. and S.B.; writing—review and editing, D.K., J.S.J., H.N., E.K. and S.B. ; visualization, D.K., J.S.J. and H.N..; supervision, D.K. and S.B.; project administration, D.K., E.K. and S.B.; funding acquisition, E.K. All authors have read and agreed to the published version of the manuscript.

Funding: This research was funded by Ferring Pharmaceuticals and its affiliates.

Data Availability Statement: Crystallographic coordinates and structure factors have been deposited to the Protein Data Bank (www.rcsb.org) as PDB ID 9XYD.

Conflicts of Interest: The authors DK., S.B., H.N. and E.K. are employees of Ferring Pharmaceuticals/BTG, a Ferring Pharmaceuticals Company. The results of this publication were derived/discovered as a result of work performed for Ferring Pharmaceuticals. The authors have no other conflicts of interest to declare.

Abbreviations

The following abbreviations are used in this manuscript:

cAMP	Cyclic adenosine-monophosphate
CG	Choriogonadotropin
ESI-MS	Electrospray ionization mass spectrometry
FSHR	FSH receptor
GC	Granulosa cells
GnRH	Gonadotropin-releasing hormone
HF	Hydrogen fluoride
LH	Luteinizing hormone
rFSH	Recombinant follicle stimulating hormone
SEC	Size exclusion column

 doi:10.20944/preprints202601.1983.v1

ST3	α2,3-sialyltransferase
VHH	Anti-kappa nanobody

References

1. Ulloa-Aguirre A. Structure-function relationship of follicle-stimulating hormone and its receptor. Hum Reprod Update. 1998;4:260–83. https://doi.org/10.1093/humupd/4.3.260
2. Leão R de BF, Esteves SC. Gonadotropin therapy in assisted reproduction: an evolutionary perspective from biologics to biotech. Clinics. 2014;69:279–93. https://doi.org/10.6061/clinics/2014(04)10
3. Bosnjak I, Bojovic V, Segvic-Bubic T, Bielen A. Occurrence of protein disulfide bonds in different domains of life: a comparison of proteins from the Protein Data Bank. Protein Engineering Design and Selection. 2014;27:65–72. https://doi.org/10.1093/protein/gzt063
4. Feige MJ, Braakman I, Hendershot LM. CHAPTER 1.1. Disulfide Bonds in Protein Folding and Stability. 2018. p. 1–33. https://doi.org/10.1039/9781788013253-00001
5. Ulloa-Aguirre A, Timossi C, Damián-Matsumura P, Dias JA. Role of Glycosylation in Function of Follicle-Stimulating Hormone. Endocrine. 1999;11:205–16. https://doi.org/10.1385/ENDO:11:3:205
6. Zhang L, Xu H, Chen C-L, Green-Church KB, Freitas MA, Chen Y-R. Mass spectrometry profiles superoxide-induced intramolecular disulfide in the FMN-binding subunit of mitochondrial complex I. J Am Soc Mass Spectrom. 2008;19:1875–86. https://doi.org/10.1016/j.jasms.2008.08.004
7. Gorman JJ, Wallis TP, Pitt JJ. Protein disulfide bond determination by mass spectrometry. Mass Spectrom Rev. 2002;21:183–216. https://doi.org/10.1002/mas.10025
8. CHMP. ANNEX I SUMMARY OF PRODUCT CHARACTERISTICS.
9. Bosch E, Havelock J, Martin FS, Rasmussen BB, Klein BM, Mannaerts B, et al. Follitropin delta in repeated ovarian stimulation for IVF: a controlled, assessor-blind Phase 3 safety trial. Reprod Biomed Online. 2019;38:195–205. https://doi.org/10.1016/j.rbmo.2018.10.012
10. Nyboe Andersen A, Nelson SM, Fauser BCJM, García-Velasco JA, Klein BM, Arce J-C, et al. Individualized versus conventional ovarian stimulation for in vitro fertilization: a multicenter, randomized, controlled, assessor-blinded, phase 3 noninferiority trial. Fertil Steril. 2017;107:387-396.e4. https://doi.org/10.1016/j.fertnstert.2016.10.033
11. US9771407.
12. Tegoni M, Spinelli S, Verhoeyen M, Davis P, Cambillau C. Crystal structure of a ternary complex between human chorionic gonadotropin (hCG) and two Fv fragments specific for the α and β-subunits 1 1Edited by I. A. Wilson. J Mol Biol. 1999;289:1375–85. https://doi.org/10.1006/jmbi.1999.2845
13. Zhang Z, Lin X, Wei L, Wu Y, Xu L, Wu L, et al. A framework for Frizzled-G protein coupling and implications to the PCP signaling pathways. Cell Discov. 2024;10:3. https://doi.org/10.1038/s41421-023-00627-y
14. Bloch JS, Mukherjee S, Kowal J, Filippova E V., Niederer M, Pardon E, et al. Development of a universal nanobody-binding Fab module for fiducial-assisted cryo-EM studies of membrane proteins. Proceedings of the National Academy of Sciences. 2021;118. https://doi.org/10.1073/pnas.2115435118
15. Fan QR, Hendrickson WA. Structure of human follicle-stimulating hormone in complex with its receptor. Nature. 2005;433:269–77. https://doi.org/10.1038/nature03206
16. Lakbub JC, Shipman JT, Desaire H. Recent mass spectrometry-based techniques and considerations for disulfide bond characterization in proteins. Anal Bioanal Chem. 2018;410:2467–84. https://doi.org/10.1007/s00216-017-0772-1
17. Fox KM, Dias JA, Van Roey P. Three-Dimensional Structure of Human Follicle-Stimulating Hormone. Molecular Endocrinology. 2001;15:378–89. https://doi.org/10.1210/mend.15.3.0603
18. Wu H, Lustbader JW, Liu Y, Canfield RE, Hendrickson WA. Structure of human chorionic gonadotropin at 2.6 å resolution from MAD analysis of the selenomethionyl protein. Structure. 1994;2:545–58. https://doi.org/10.1016/S0969-2126(00)00054-X

 doi:10.20944/preprints202601.1983.v1

19. Lapthorn AJ, Harris DC, Littlejohn A, Lustbader JW, Canfield RE, Machin KJ, et al. Crystal structure of human chorionic gonadotropin. Nature. 1994;369:455–61. https://doi.org/10.1038/369455a0
20. Lustbader JW, Birken S, Pileggi NF, Kolks MAG, Pollak S, Cuff ME, et al. Crystallization and characterization of human chorionic gonadotropin in chemically deglycosylated and enzymically desialylated states. Biochemistry. 1989;28:9239–43. https://doi.org/10.1021/bi00450a001